Single-Layer, Flexible, and Depolarizing Chipless RFID Tags

Angel Ramos, Zeshan Ali, Arnaud Vena, Marco Garbati, Etienne Perret

Single-layer, Flexible, and Depolarizing Chipless RFID Tags

Angel Ramos[1], Zeshan Ali[1], Arnaud Vena[2], Marco Garbati[1] and Etienne Perret[1, 3], Senior Member, IEEE

[1]Univ. Grenoble Alpes, Grenoble INP, LCIS, 26000 Valence, France
[2]Université de Montpellier, Institut d'Electronique et Systèmes (IES), 34095 Montpellier, France
[3]Institut Universitaire de France, 75005 Paris, France

Corresponding author: zeshan ali (e-mail: zeshan.ali@lcis.grenoble-inp.fr).

This work was supported by the Institut Universitaire de France.

ABSTRACT This work presents the designs of single-layer chipless radio frequency identification (RFID) tags based on the RF-encoding particles (REP) approach. These tags are the first realized for reading in cross-polarization resulting in a higher immunity against multipath, and thus, achieving robust readings in a practical environment. The proposed chipless tags are of credit-card size, operating in the ultra-wideband (UWB) ranging from 3.1 GHz to 10.6 GHz, compliant with low-cost additive fabrication techniques, and realized with low-cost plastic and paper substrates. A study on the reader-tag polarization and rotation angle is performed for the proposed designs and compared with existing designs of two-layers. For the first time, it is presented that the low-cost single-layer tags can be read in realistic environments with only one measurement.

INDEX TERMS Chipless, Depolarizing, Frequency-Coded, RFID, Single-Layer

I. INTRODUCTION

Chipless radio frequency (RF) identification (RFID) systems have been the subject of many studies for years because of their potential low-cost compared to classical chip-based RFID approaches [1], [2]. The main advantage of chipless RFID is that the cost of the tags can significantly be reduced because of the absence of the integrated circuit (IC) or chip containing the identification information on tag. This characteristic of operation without a chip results in that the tags can be realized entirely by means of printed electronics [3], [4]. With a single-layer tag design, flexibility in the fabrication process of chipless tags and barcodes is comparable, where conductive ink is required for the fabrication of chipless tags instead of the ordinary ink.

Recently, several approaches have been proposed to encode the information in chipless RFID. Time-coded tags encode their ID in the delay between two reflected peaks [5]. Frequency-coded tags encode their ID in the presence or absence of frequency absorptions or frequency peaks [6]. Other approaches encode their ID in group delay of coupled C-sections [7]. In general, the main advantage of time-coded over frequency-coded tags is the robustness of detection. Frequency-coded tags, however, can encode a larger number of bits, at the cost of larger tag sizes and shorter read-ranges.

Depolarizing chipless RFID tags discussed in [8], [9] provide the cross-polarization tag response. The cross-polarization tag response exhibits only a limited contribution of unknown surrounding objects (see [8, eq. (9)]). On the contrary, the co-polarization tag response is dependent on unknown surrounding objects response (see [8, eq. (8)]). Such independence from unknown surrounding objects in cross-polarization makes it more reliable and suitable for practical implementation of the chipless RFID technology. Even with this advancement, chipless tags should also be able to operate when directly printed on different practical substrates (i.e., paper, and cardboard). In this regard, single-layer chipless frequency-coded tags have been introduced recently. The absence of a ground plane in frequency-coded tags can cause difficulties in reading them in realistic industrial applications, where the tag is directly in contact with an unknown material, such as metal or lossy objects. Some works [10], [11] have proposed techniques to compensate for the detuning effect caused by the medium permittivity variation due to the presence of an unknown object. Alternatively, a single-layer tag can be used as a

Angel Ramos is now with Qorvo Inc., 3511 Utrecht, The Netherlands.

sensor [12], [13]. The tag can be in contact with the material under evaluation, and the reading can be done from both sides of the tag due to the absence of a ground plane. In [12], a single-layer humidity UHF RFID chipless sensor tag is presented along with wired measurements on paper substrate.

Table I summarizes the state of the art of single-layer chipless RFID tags to increase the coding capacity [14]–[16], orientation independence [14], [17]–[19], size miniaturization [20], dielectric sensing [21], and imaging [22]. However, in most of these works [14]–[22], chipless tags are realized on high-performance expensive copper laminated substrates except in [17], [22], where 3-D printing technology and photolithography are used, respectively. Furthermore, these works [14]–[22] are based on two measurements approach (i.e., one in the presence of tag and second in the absence of tag) which is not suitable for practical scenarios. Particularly, the supplementary background measurement (i.e., in the absence of tag) would not be valid when the objects in the background environment are moving.

TABLE I
STATE OF THE ART OF SINGLE-LAYER CHIPLESS RFID TAGS

Shape of resonator	Polarization of reading	Type of substrate	Measurement approach
I-shaped [14]	Co	Taconic TLX-8 ($\tan\delta \approx 0.0017$)	Two measurements
U-shaped [15], [20]	Co	Taconic TLX-0 ($\tan\delta \approx 0.0019$)	Two measurements
Rectangular ring [16]	Co	F4BM ($\tan\delta \approx 0.0007$)	Two measurements
Circular ring [17]	Co	Taconic TLX-9 ($\tan\delta \approx 0.0019$)	Two measurements
Trefoil-shaped [18]	Co	Rogers 5880 ($\tan\delta \approx 0.0009$)	Two measurements
L-shaped [19]	Co	Rogers 5880 ($\tan\delta \approx 0.0009$)	Two measurements
45° inclined dipole [21]	Cross	Rogers 4003 ($\tan\delta \approx 0.0025$)	Two measurements
45° inclined dipole and meandered dipole [22]	Cross	Taconic TLX-8 ($\tan\delta \approx 0.0017$) Paper†	Two measurements
L-shaped (This Work)	Cross	PET ($\tan\delta \approx 0.002$) Paper‡ ($\tan\delta \approx 0.12$)	Single measurement

† Loss is not mentioned
‡ Lossy substrate

Indeed, the current demands in the field of chipless RFID technology are the miniaturization of the size, increasing the coding capacity, and orientation independence. However, these advancements would not be beneficial without robust reading of chipless tags, which is the focus of this manuscript. The encoding bandwidth of a resonator is dependent on its quality factor *Q*. For high coding capacity, each resonator in the design of chipless tag should be sufficiently selective presenting a sufficiently high *Q* so that larger number of peaks can be accommodated in a defined bandwidth. Such highly selective peaks can be achieved by: (i) improving the design of the resonator (e.g., coupling multiple elements). (ii) choosing a low loss substrate. (iii) incorporating the ground plane in the design of chipless tag (dual-layer design with higher quality factor *Q*). However, practical implementation of chipless RFID technology for item-level tagging implies the compact single-layer design of chipless tag printed on low-cost substrates (e.g., plastic, cardboard or paper). Practically, compactness of chipless tag and proximate coupling restrict number of coding resonators [8]. On the other hand, the high dielectric losses ($1/Q_d$) in low-cost substrates, the significant conduction losses ($1/Q_c$) in the printed layer of conductive ink (as compared to copper-coated layer), and the radiation losses ($1/Q_r$) due to the presence of multiple resonators in the design of chipless tag limit the overall quality factor *Q* [3]:

$$\frac{1}{Q} = \frac{1}{Q_d} + \frac{1}{Q_c} + \frac{1}{Q_r} \quad (1)$$

where $Q_d = 1/\tan\delta$. As the quality factor of the resonators used in the design of tag is reduced, the frequency peaks used to encode information are more difficult to identify [23]. Therefore, the practical implementation of chipless RFID requires robustness of tag reading, where inkjet printing on low-cost substrates also imposed a tradeoff between the size of the tag (due multiple scatterers) and the coding capacity.

To lower the tag cost and for ease of use for industrial applications, two designs of L-shaped resonators based chipless single-layer tags on plastic substrate, fabricated with additive techniques, and based on cross-polarization principle (depolarizing principle) are proposed for the first time through this paper. Like in [8], [14], [15], the tag is based on RF-encoding particles (REP) approach and thus, composed of only resonators used to encode information. In this paper, contrary to works in [15], [20], the tag is designed to rotate the polarization angle of the reader's incoming signal by virtue of the absence of plane of symmetry regarding the polarization of the incident E-field. Thus, the tag is read in cross-polarization, adding robust detection capabilities in front of nearby objects. Contrary to previous studies of single-layer chipless tag, only one cross-polarized measurement is used instead of several (one measurement at each polarization, plus one or two measurements for calibration). A proof-of-concept paper tag is also proposed using the same structure, showing that the solution might be extended to paper if substrate losses could be minimized. The cross polarization tag reading based studies (i.e., close to our work) [21] and [22] are focused primarily on sensing and imaging, respectively. To the best of authors' knowledge single-layer depolarizing chipless tags realized on a low-cost lossy substrate characterized in a cross-polarization environment with single measurement approach have not been studied before.

The orientation angle in which the tag is read is the main concern in both chip-based [24] and chipless RFID systems

[14], [25]. Since the radiating element(s) in a tag are not ideally isotropic, there might be tag-reader illumination angles where a proper reading cannot be obtained. This work also studied the effects of variation of the tag-reader orientation (both in E and H planes) on the reading of the proposed tags. Our work can be differentiated from the existing works on slot L-shaped resonators [19], as it is designed on high-performance substrate and measured in co-polarization with two measurements approach. Also, most of the presented analyses (e.g., effects of rotation, metals inks, and direction of tag reading) are based merely on simulations results.

This paper is organized as follows. Section II presents the operating theory and the design of single-layer depolarizing tags. Section III presents simulations and compares single- and dual-layer depolarizing chipless tags with similar co-polarization tags. Section IV presents performance measurements of the proposed tags in several scenarios. Section V performs a study on the incidence angle between the reader and the tag. Finally, Section VI draws the conclusions.

II. THEORY AND TAG DESIGN

A. CHIPLESS TAGS WITHOUT GROUND PLANE CHALLENGES

The presence of a ground plane on a tag changes the characteristics of a resonance scatterer considerably. The design with a ground plane on the rear side of a tag greatly eases its detection. It isolates the tag electromagnetically from the object at which it is attached, and eases the design of scatterers with high quality factor. This is particularly true for chipless tags realized with RF-encoding particles. These REPs act as a transmitting/receiving antenna and a filtering circuit [1]. Each REP creates a peak on the received wideband signal at a frequency that depends on each REP's dimensions, but mostly on the technology used to implement these resonant circuits.

Resonant circuits are of great importance in RF [26]. In the frequency range corresponding to the proposed application (UWB, from 3.1 to 10.6 GHz), microwave cavities have the highest quality factor and thus, would be the most suitable. However, microwave cavities cannot keep the system low-cost. In chipless RFID, one of the more suitable solutions is to consider a microstrip patch antenna as a scatterer [27]. There are several advantages in using microstrip technology, including:

- Microstrip patches are used as antennas to ensure good radiation efficiency and thus, a high radar cross-section (RCS).
- It is compact, planar, and compatible with low-cost fabrication.
- It behaves similarly to a cavity and is thus, narrow bandwidth [28]. This permits better selectivity in the frequency domain, and thus, affords more possible identification codes.
- It is well known and formulas for design are available in the literature.

For these reasons, microstrip technology was chosen in [8], [10], [11], [29] for the design of the elementary coding particles. In [10], different shapes of a microstrip patch (rectangular, circular, elliptic, etc.) have been simulated. The evolution of its quality factor with respect to the frequency of resonance has been evaluated and compared. Note that for a resonance occurring at the same frequency, the shape of the resonator adds little effect on the quality factor. In microstrip technology, the ground plane plays a major role in the quality factor of the particles [11]. For instance, coupled microstrip dipoles with ground plane [8] have a quality factor in the order of 140 at 4.4 GHz [11]. Without ground plane, a quality factor less than 5 can be obtained at the same resonant frequency for a dipole shape. This drop of quality factor shows that the dipole without a ground plane is much less selective in frequency than the coupled dipole with a ground plane, making it practically impossible to encode information in a resonant frequency peak [23]. To increase the quality factor, single-layer REP particles need to be implemented using the transmission line technology. One of the most employed particles is the C-folded dipole, which is based on a coplanar strip (CPS) line with one end in short circuit and the other in open circuit [10]. A CPS line with the two ends in short circuit can also be used [14]. These resonators based on transmission lines can achieve a much higher quality factor than the single-layer dipoles previously considered. Indeed, the quality factor of the C-folded dipole is around 40 at 4.4 GHz. Still, this quality factor is significantly lower than the one for the coupled microstrip dipoles with ground plane (approximately 140). This explains the difficulty of designing single-layer depolarizing chipless tags.

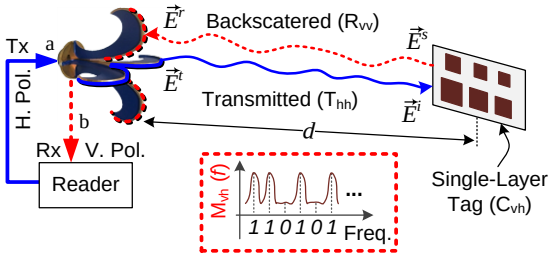

FIGURE 1. Scheme of the tag-reader system.

B. DEPOLARIZING APPROACH ON A SINGLE-LAYER TAG

To improve detection, a chipless tag has to be designed to work in cross-polarization (depolarization). Fig. 1 shows a scheme of a depolarizing chipless RFID system [8] along with the signals involved. The reader transmits a horizontally polarized (*h*) signal through its transmitting (Tx) antenna. Then, the tag reflects (backscatters) a vertically polarized (*v*) signal, which is received through the reader's receiving (Rx)

antenna. The tags are composed of REPs designed to change the polarization of the incoming wave. With this practice, the reader works in cross-polarization decreasing the multipath effects. In fact, nearby objects to the tag are not designed to specifically cross the polarization of the incoming EM wave. In Fig. 1, E^t and E^r denote the transmitted and received electric fields at the reader, respectively. Similarly, E^i and E^s denote the incoming and backscattered fields at the tag, respectively. A block diagram of the detection system has been introduced in [8, Fig. 5]. From [8], the cross-polarized signal M_{vh} received by the reader can be approximated as:

$$M_{vh} \approx I_{vh} + R_{vv} C_{vh} T_{hh}, \tag{2}$$

where I_{vh} is the measured signal without the presence of the tag and the object. I_{vh} is also addressed as empty measurement or isolation. R_{vv} is the received path in vertical polarization, C_{vh} is the tag response in cross-polarization, and T_{hh} is the transmitted path in horizontal polarization. Formula (2) is intended for depolarizing tags with ground plane. This is because the ground plane is able to isolate the tag from the attached object electromagnetically. For a single-layer chipless tag, formula (2) can still be used, but in C_{vh}, the tag's resonators are influenced by effective permittivity with the attached object [30]. Its effects may be compensated with detuning correction technique [31].

Formula (2) expects a cross-polarization contribution of the environment much lower than that of the tag ($R_{vv} C_{vh} T_{hh}$) and it has been proven for ground plane tag [8]. The question now is if such approximation can still be considered in the case of single-layer depolarizing tags. As an example, consider a tag with a ground plane (quality factor of 140) [10] and an ungrounded tag with a lower quality factor of 40 [11] chipless tags. The environment is composed of a wooden slab (i.e., CARP, $\varepsilon_r = 5.7$), 1 cm thick, and with a 30 cm² surface. Note that from an analytical point of view, by considering a second order transfer function which is used to fit the REP scatterers around their frequencies of resonance f_r [11], the magnitude of the peak apex at f_r can be calculated as:

$$G(f_r) = \frac{Q}{\sqrt{1 - \left(\frac{1}{2Q}\right)^2}}, \tag{3}$$

where a transfer function with unity gain at DC has been used, and Q is the quality factor of the scatterer. In (3), substituting Q with 40 and 140, the magnitude of the peak apex observed for the ungrounded tag is around 5 dB lower than the grounded configuration. This was confirmed by simulation in [8], where the RCS of this grounded tag C_{vh}^{g} was around -24.9 dB [8] at 4.2 GHz, and the RCS of a single-layer tag C_{vh}^{ung} was around -29.3 dB at 4.4 GHz. Considering d = 30 cm in Fig. 1, the signal level of the wooden slab is around -60 dB, that is to say, 15 dB lower than the term $\left|R_{vv} C_{vh}^{ung} T_{hh}\right|$ corresponding to the single-layer tag around its resonance frequencies. Several configurations varying the distance d and the slab material have been tested; always, a clear magnitude separation of more than 10 dB has been observed in practice. This shows that for depolarizing chipless tags with or without a ground plane, it is possible to use formula (2).

To retrieve the tag ID, that is, to extract $R_{vv} C_{vh} T_{hh}$ from (2) using a single measurement, a temporal separation technique can be implemented like in [23] to remove I_{vh}. However, due to the reduction of the quality factor compared to the grounded tag [23], a specific study has to be done as detailed in the next section.

C. TAG DESIGN

A depolarized tag is composed of several resonant scatterers. Contrary to non-depolarized tags, at the resonance, the orientation of the current paths on the conductors of these resonators are not restricted to be parallel to the incident wave. This means that there are generated current paths in the orthogonal direction to the incident wave that are at the origin of the backscattered wave in cross-polarization. To obtain such specifications, it is necessary to create an asymmetry (as regards the incident field orientation) in the resonator geometry. The two proposed tags are shown in Fig. 2 and are composed of asymmetric slots that enable the generation of the cross-polarization signal. The two depolarizing tags are single-layer and based on REP approach.

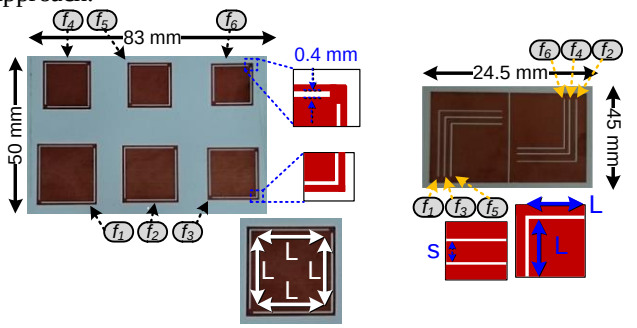

(a) (b)

FIGURE 2. Photograph of the proposed single-layer chipless depolarizing tags: (a) design A and (b) design B.

The tags are fabricated by a two-step additive process of patterning and metallization [32]. Their size fits inside a reference credit card of 85.60 × 53.98 mm^2. The plastic substrate is flexible polyethylene terephthalate (PET) with permittivity $\varepsilon_r = 3.55$, loss tangent of 0.002, and height of 0.1 mm. The top layer conductor is copper with a thickness of 35 µm. The design dimensions L are calculated so that the corresponding resonant frequencies appear within 3 and 6 GHz.

The resonant frequency of each REP is changed by the length L of an L-shaped slot in the copper plane and is calculated so that the corresponding resonant frequencies appear within 3 and 6 GHz. The slots are 0.4-mm wide, which is sufficient for the fabrication resolution while

keeping a narrow slot (higher Q factor) [33]. Design A is composed of six particles with two slots each, while Design B is composed of six slots each resonating at a precise frequency in the band of interest. Design A is more robust because the tag has two identical symmetrical slots for each REP. The addition of a second slot tends to increase the magnitude level of the peak. Indeed, by increasing the number of slots, it is possible to increase the quality factor and the backscattered E-field as shown in (3). Design B is more compact and the separation s between slots is higher than 1 mm to minimize the coupling between them.

Non-depolarizing U-shaped slot resonators in [15] are appropriate for the co-polarization tag reading configuration, as shown in Fig. 3(a). This behavior is because of the plane of symmetry of the resonator. For an ideal co-polarization tag reading configuration, Tx and Rx would always be parallel to the plane of symmetry. Such a resonator might not be employed the tag reading in cross-polarization unless it is rotated at an angle of 45°. The novelty of the proposed designs is the absence of plane of symmetry in the direction of the incident E field, that is, precisely appropriate for the cross-polarization tag reading configuration. For example, design A is shown in Fig. 3(b).

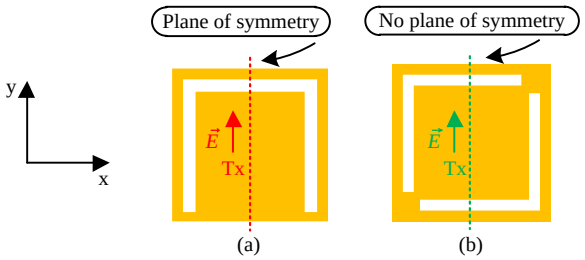

FIGURE 3. Illustration of plane of symmetry. (a) Non-depolarizing U-shaped slot resonator [15]. (b) Proposed depolarizing design A.

III. SIMULATION AND COMPARISON WITH DUAL-LAYER DESIGNS

The tags were simulated in CST Microwave Studio (time domain solver), with a plane wave and a cross-polarized E-field (far field) probe at a 20 cm distance. The frequency was between 1 and 10 GHz, and the simulation time was up to 25 ns. The simulated current densities for both tag's designs are shown in Fig. 4. The current is concentrated around the edges of the slots showing a perpendicular contribution that originates from the cross-polarized reflected EM wave. Both designs have similar current densities, with peaks at around 0.165 A/m^2.

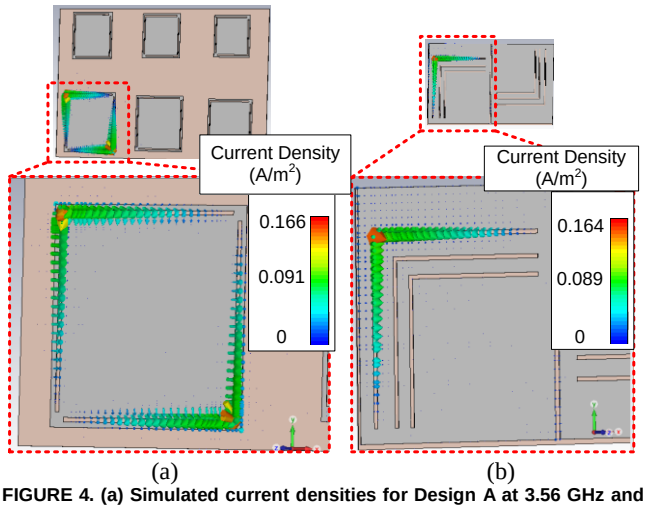

FIGURE 4. (a) Simulated current densities for Design A at 3.56 GHz and (b) Design B at 3.45 GHz.

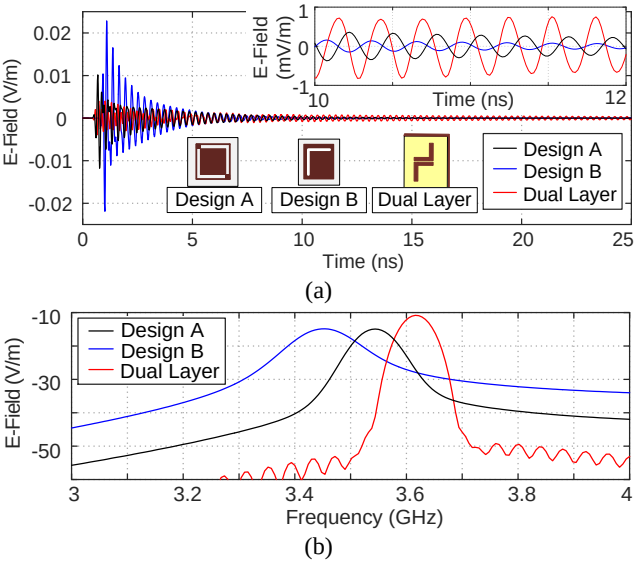

FIGURE 5. (a) Simulated cross-polarization time and (b) frequency domain response of one resonator of the proposed single-layer designs, as well as a dual-layer case.

Since the tag does not have a ground plane, the object where the tag is attached is not well isolated (even though the tag works in cross-polarization). The flexible plastic substrate used, which is not specifically designed for RF, also degrades the tag's performance. Moreover, the time duration of the tag response is short due to the lack of ground plane and low quality factor. In consequence, a time-windowing signal processing method is not as easily applicable as for a tag with ground plane to eliminate I_{vh} from (2). To study this, Fig. 5 shows the time and frequency domain response of one of the resonators (highlighted in Fig. 4) for both proposed designs. For comparison purposes, one resonator of a dual-layer tag [8] with a similar structure and frequency is also shown. The energy exponential decay of the proposed tags is more accentuated than that of the dual-layer tag. Since Design A has a redundant shape (two slots for resonant frequency), its quality factor is higher, which makes it more suitable for

detection. Indeed, the decrease of the quality factor has two main effects on the scatterer's response: a larger bandwidth of the peaks and a resonance of lower intensity [see formula (3)]. The former limits the bit capacity of the tag as it is necessary to use a larger spacing between two consecutive peaks to avoid potential interference. The latter results in a lower magnitude of the peaks, and this continues to hold true as the frequency increases [11].

IV. MEASUREMENT RESULT

A. CHIPLESS TAG REALIZED ON PLASTIC SUBSTRATE

An Agilent N5224A vector network analyzer (VNA) was used to characterize the proposed tags [8]. Ports 1 and 2 were connected, respectively, to the horizontal and vertical polarizations of the dual-polarized Satimo QH2000 wideband antenna. The VNA was swept from 3 to 10 GHz with 6401 points and +0 dBm of output power. Each measurement was obtained from the transmission coefficient S_{21} parameter.

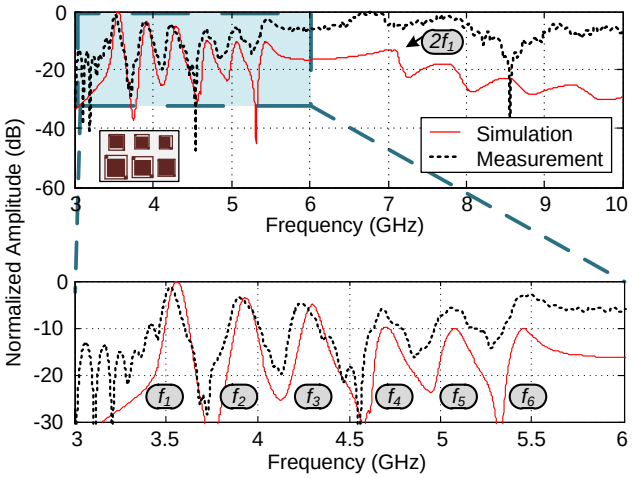

FIGURE 6. Comparison between the simulated and measured frequency-domain responses of tag Design A, inside an anechoic chamber using a background (empty-room) subtraction. Tag-reader distance: 25 cm.

To compare with simulation results, the first measurements were realized in an anechoic chamber without any high permittivity object surrounding the tag. The measurement was performed at a tag-reader distance of 25 cm, with the tag attached to a foam ($\varepsilon_r \approx 1.1$) used as support. To remove the contribution of the coupling between the two antennas [I_{vh} in (2)], a background measurement (empty-room response, i.e., measurement of the scene without the presence of the tag) was also performed, and subtracted from the tag measurement. The comparison between the simulation and measurement of design A is shown in Fig. 6. It shows a small frequency shift due to the small permittivity difference in the foam with respect to the air simulated case ($\varepsilon_r = 1$), and also due to small tolerances in fabrication. Nevertheless, all resonances can be detected. The same measurement is shown for design B in Fig. 7. In this case, as explained in Section III, the detection is more difficult because the L-shaped slots are not duplicated.

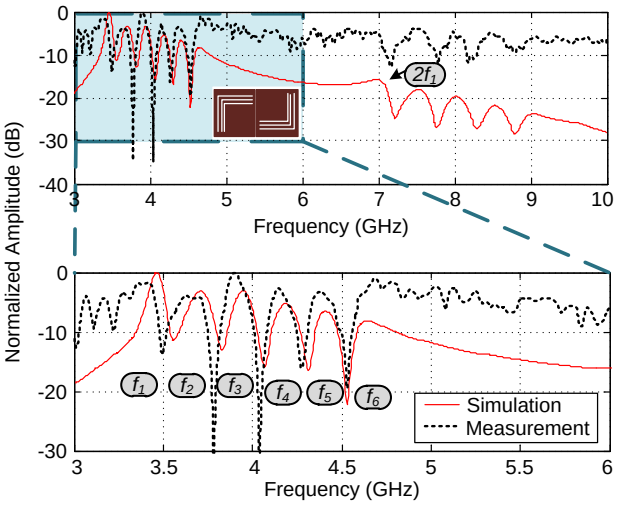

FIGURE 7. Comparison between the simulated and measured frequency-domain response of tag Design B, inside an anechoic chamber using a background (empty-room) subtraction. Tag-reader distance: 25 cm.

B. SINGLE MEASUREMENT APPROACH

To read the tag using only one measurement, a time separation approach was used in post-processing over the measurement with the tag [23] (the background measurement was not used at all). The time-domain signal was obtained from the inverse Fourier transform of the measured S_{21} parameter, with a window from 0.1 to 30 ns. Then, the short-time Fourier transform (STFT) was applied to calculate the spectrogram of the signal. For each delay τ, the Fourier transform of the signal in time with a window of $T = 12$ ns was calculated for each step. Contrary to advanced methods like the ones based on singularity expansion method (SEM) [34]–[36], the STFT can be computed rapidly with fast Fourier transform (FFT) algorithm which is less time-consuming, and compatible with real-time chipless reading applications. The calculated spectrogram using the specified parameters for Design A is shown in Fig. 8(a). There is an area, marked in green, where the resonances associated with the tag are more visible. By averaging the spectrogram along τ axis in this area, it is possible to increase the signal to noise (S/N) ratio of the measurement underlining the redundant information represented by the tag resonances. The averaged spectrogram is shown in Fig. 8(b).

To provide more results, two more tags of Designs A and B were realized and labeled with tag 2 and tag 3, respectively. Tags 2 and 3 have small differences in the length L of some of their REPs, and hence, their resonant frequency is slightly changed. The same single measurement process with time separation approach was used to read the newly realized tags in anechoic chamber. The normalized averaged spectrograms for the three tags of Designs A and B are shown in Fig. 9 and Fig. 10, respectively. In Fig. 10, the detection is more difficult due to the presence of only one

slot for resonator [14]. The single measurement approach demonstrates that even without calibration, the tag ID can still be recovered. Among others, this proves that frequency shift coding is robust against reader antenna gain variation (in our case, few dB of variation into the used frequency range). Also, it is demonstrated that contrary to what has been done in [23], temporal separation can also be applied on low quality factor single-layer depolarizing tags when the calculation parameters are finely tuned.

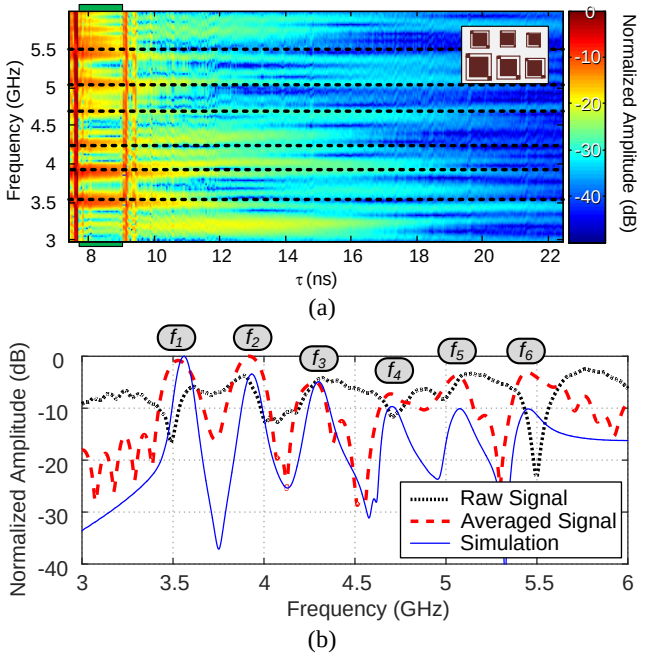

FIGURE 8. (a) STFT spectrogram of Design A measurement (without background subtraction) at 25 cm inside an anechoic chamber. In green: area used for averaging. (b) Comparison between averaged and raw signals, both without background subtraction.

The coding used was based on the frequency shift technique already used in [8]. In both cases A and B, the number of REPs was equal to 6. According to the measurement results shown in Figs. 6 and 7, a frequency resolution that is equal to the bandwidth of a resonant peak may be defined. For Design A, a resolution bandwidth close to 100 MHz was observed. The total bandwidth was 2.5 GHz from 3.5 to 6 GHz. This led to a frequency window of 400 MHz for each resonator. According to [8, eq. (13)], four different combinations for each resonator were obtained, giving a total number of combinations equals to $4^6 = 4096$, that is, 13 bits.

For Design B, according to Fig. 7, the frequency resolution is close to 100 MHz. The chosen total bandwidth was intentionally limited to 1250 MHz from 3.5 to 4.75 GHz so that the frequency window was 250 MHz for each resonator.

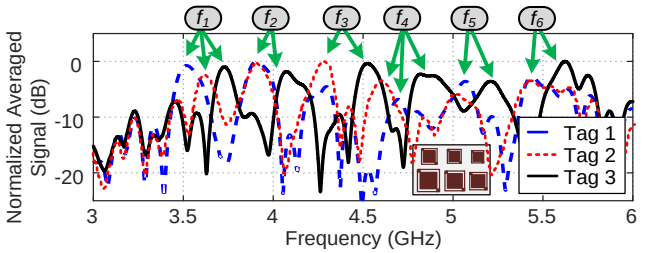

FIGURE 9. Normalized averaged signal of Design A STFT spectrogram, without background and at 25 cm inside an anechoic chamber. Three different tags are shown, where the design dimension L has been modified to change their resonant frequencies.

Using [8, eq. (13)], three different combinations for each resonance were obtained, and a total coding capacity of $N=3^6= 729$, that is 9.5 bits. In comparison with Design A, its lower quality factor makes its scatterers difficult to be used at a frequency higher than 4.75 GHz. It holds true when the measurement is obtained in a real environment.

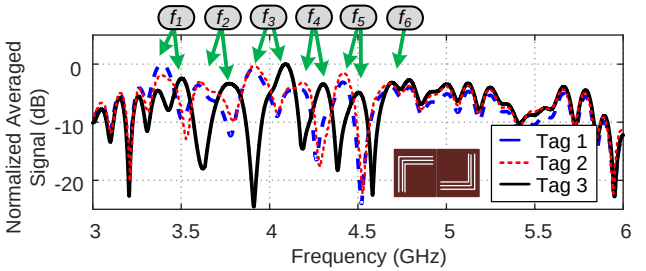

FIGURE 10. Normalized averaged signal of Design B STFT spectrogram, without background subtraction and at 25 cm inside an anechoic chamber. Three different tags are shown, where the design dimension L has been modified to change their resonant frequencies.

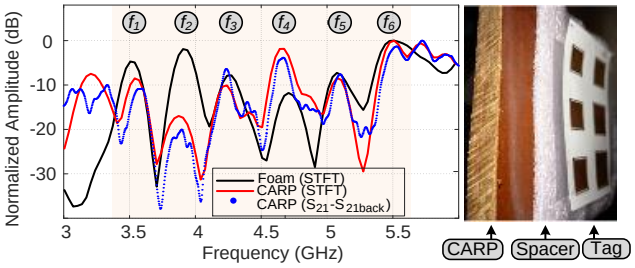

FIGURE 11. Normalized summated signal of Design A STFT spectrogram, without background at 25 cm inside an anechoic chamber. A material (CARP slab with ε_r = 5) is attached on the back of the tag. The same measurement without the STFT spectrogram and with background substation is given for comparison.

To test the tag behavior on different materials, a wood slab (CARP, ε_r = 5.7) of 1 cm thickness was attached on the back face of tag Design A. A thin foam spacer of 2 mm was also added in order to not modify the tag's substrate permittivity and losses. The result using the single measurement reading technique is shown in Fig. 11. It shows that the tag is successfully detected when attached to the material. On the other hand, the result using the background subtraction (see Fig. 11) is comparable with the single measurement reading technique result. With the use of the thin foam spacer, the resonant frequencies were not greatly modified, and though

possible, no compensation method was required, as it was performed in [10].

C. MEASUREMENT IN A PRACTICAL ENVIRONMENT

A tag using Design A was measured in a real environment. From a previous study (Fig. 8), the temporal process based on the spectrogram provided more exploitable results whatever was the measurement configuration considered. Therefore, this post-processing technique was used for the rest of the article. To compare the performance of the proposed tags with single-layer tags realized in co-polarization [10], two more tags were fabricated with the same procedure described in Section II. For the purpose of comparison, both single and background subtraction measurement techniques were used as the reading process. The measurement result of the three tags is shown in Fig. 12. The "Reference" signal is with the background subtraction technique, while the "Averaged Sig." signals are calculated with the single measurement. From Fig. 12(a) and 12(b), the single-layer depolarizing tag proposed here can be read successfully. Under the same exact conditions, however, the co-polarization tags cannot be read [Figs. 12(c), (d), (e) and (f)]. In the best case, Fig. 12(e), the four tag's resonances are present, but several unwanted peaks prevent any reading. Fig. 12(g) shows the measurement setup in a real environment.

From these measurements, the improvement with the depolarizing tag design is clearly seen. This comparison proves the robustness of these single-layer depolarizing tags. Contrary to classical co-polarization chipless tags, these new tags can be read with only one measurement which represents a great improvement for real case scenario. To our knowledge, it is the first time that a single-layer chipless tag can be read without an additional calibration measurement.

D. CHIPLESS TAG REALIZED ON PAPER SUBSTRATE

The polyethylene terephthalate (PET) substrate used for Designs A and B as well as the additive technique used in [3] already have lower cost than typically used high-performance substrates such as Rogers RO4003C with subtractive techniques [8], [25], [37]. However, chipless tags on paper substrates are also under active research because their cost is potentially the lowest possible [3], [12]. Three tags of Design B were realized as a proof-of-concept on a cellulose-based substrate. The paper substrate has a thickness of 95 µm, a relative permittivity ε_r of 3.3 and a loss tangent tanδ of 0.12. A 2.6 µm thick layer of silver conductive ink was deposited on the substrate with an ordinary inkjet printer. The manufacturer's printing process has a resolution of 15 µm, which is more than one order of magnitude better than the required gap (0.4 mm, see Fig. 2). The manufactured tag is shown in Fig. 13.

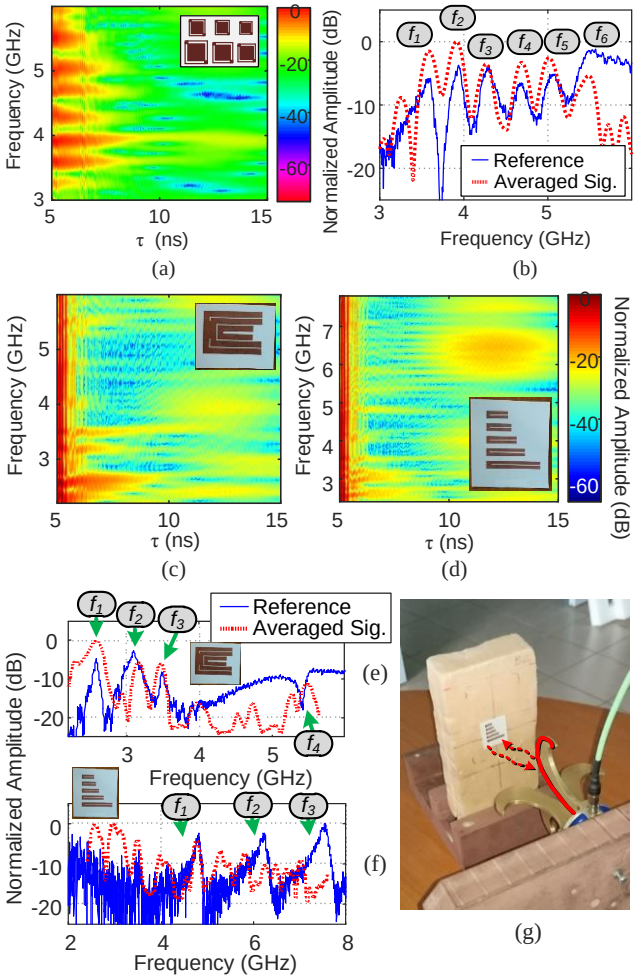

FIGURE 12. (a) STFT spectrogram of Design A without background subtraction at 15 cm in a real environment. (b) Corresponding averaged signal from (a) the spectrogram along with reference. (c) and (d): STFT spectrograms of two co-polarization tags realized with the same additive procedure and measured under the same conditions. (e) and (f): Corresponding averaged signals from (c) and (d) spectrograms along with their references. (g) Photograph of the measurement setup in a real environment with a co-polarization tag.

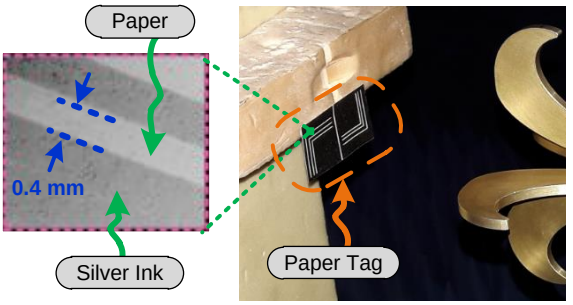

FIGURE 13. Photograph of the proof-of-concept Design B tag on paper inside an anechoic test environment.

The tags were measured with a single measurement technique inside an anechoic chamber, as shown in Fig. 13, and on top of a foam. Fig. 14 shows the STFT spectrogram of the measurements. Their corresponding normalized averaged spectrograms are shown in Fig. 15. It shows that the resonant frequencies have been shifted down with respect

to Section IV (A). This was due to the higher permittivity of the paper used. The higher resonant frequencies (f_4, f_5 and f_6) could not be detected even inside an anechoic environment due to substrate losses. Note that the losses of this substrate were two orders of magnitude above RO4003C or even the PET substrate used in Section IV(A). An in-depth study on the dielectric properties or manufacturing processes is out of the scope of this paper. Nevertheless, these results show that the proposed single-layer depolarizing designs could be extended to other types of substrates and materials if losses can be controlled. As the proposed designs are single-layer (i.e., without a ground plane), these might not be employed on metallic objects.

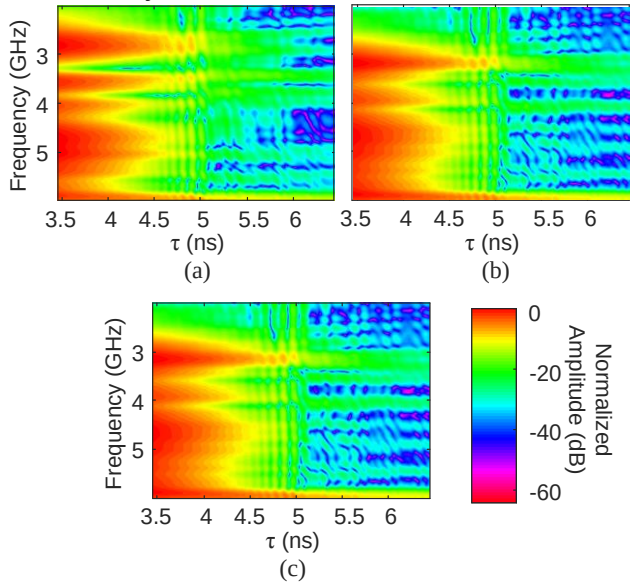

FIGURE 14. STFT spectrogram of the proof-of-concept of Design B tags 1 (a), 2 (b) and 3 (c) on paper substrate.

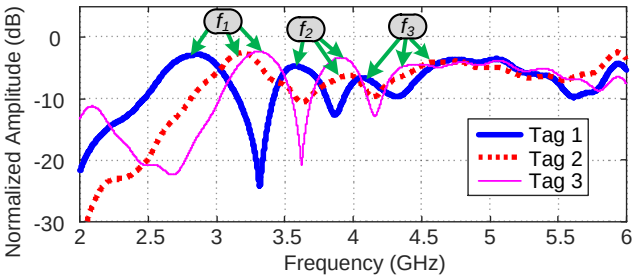

FIGURE 15. Normalized averaged signal of Design B STFT spectrograms in Fig. 14.

V. ANGULAR BEHAVIOR

A. ROTATION SETUPS

Reading a tag in any tag-reader angle is a major concern, both in polarization angle [14] and in the tag rotation [25]. This section covers the influence of the angles in E and H planes with respect to the reader antennas. To do so, two measurement setups were used (see Fig. 16). The influence of the change in E plane, that is, the change of the polarization angle corresponds to the setup in Fig. 16(a). Similarly, the tag's rotation influence (H plane) corresponds to the setup in Fig. 16(b). Design A was selected here because it is more robust than Design B (see Section IV).

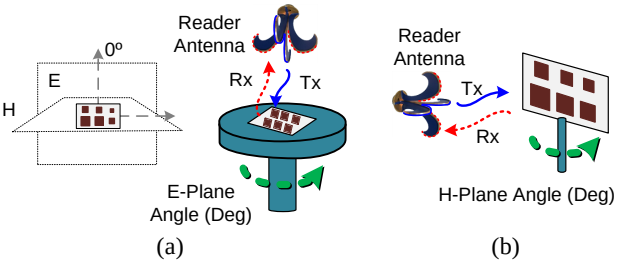

FIGURE 16. (a) Scheme of the rotation simulations and measurements in E and (b) H planes.

B. ROTATION IN E-PLANE

To maximize the power backscattered by the tag in a depolarizing approach, the orientation of the L-shaped slots has to be in accordance with the polarization of the reader's antennas. For other angles, the received power of the REPs will be decreased [38], thus, ideally, the tag should be read in multiples of 90º (i.e., 0º, 90º, 180º, and 270º). To study the intermediate cases, due to the symmetrical shape of the structure, the angle was swept from 0º to 90º in 5º steps, both in simulations and in measurement. The measurement was performed inside an anechoic chamber and both; the single measurement and background subtraction technique were used. The SEM theory has shown that the natural resonance frequency of a scatterer is aspect-independent in nature [35], [36]. A simple method to recover the natural resonance is to observe the spectrogram of the signal and to isolate the resonant part (late-time) from the specular response of the substrate (early-time) by applying a time-frequency window [see Fig. 8(a)] [29]. As the temporal separation method is based on the measurement of the natural resonances, it is robust to variations in the measurement setup such as tag rotation.

The measured frequency-domain response of Design A (tag 1) as a function of the E-plane angle is shown in Fig. 17 (a). For each angle, the peaks are obtained and the frequency shift is calculated with respect to the ideal case (0º). In Fig. 17(b), the measured resonant frequency shifts as a function of the polarization E-plane angle are shown. The proposed tags can be read at most of the angles. Analogously, Fig. 17(c) shows the normalized peak values for all the resonances. It shows that the perpendicular orientations (0º and 90º) have higher peak values and in consequence, the lowest frequency deviations.

As discussed in Section IV, for the system to work with a 100-MHz bandwidth for each resonator, the deviations must be lower than ± 50 MHz. The worst cases are around 45º [in the range 35°-55°, see the checkboard shaded area of Figs. 17(b) and (c)]. This behavior is due to polarization mismatch when E-field is around an inclination of 45º [see Fig. 3(b)]. In such cases, the backscattering signal from the tag is very low; therefore, the S/N ratio of the reading system

is too low to extract an exploitable value. Apart from these specific orientations, frequency shifts lower than 20 MHz are obtained for all the resonators. This is in good agreement with the simulation, where no variations should be observed. It is important to note the minimum resolution of frequency shift in Fig. 17(a) is 20 MHz. Therefore, for the rest of this paper, the frequency shifts of zero are in fact in a range from 0 to 20 MHz.

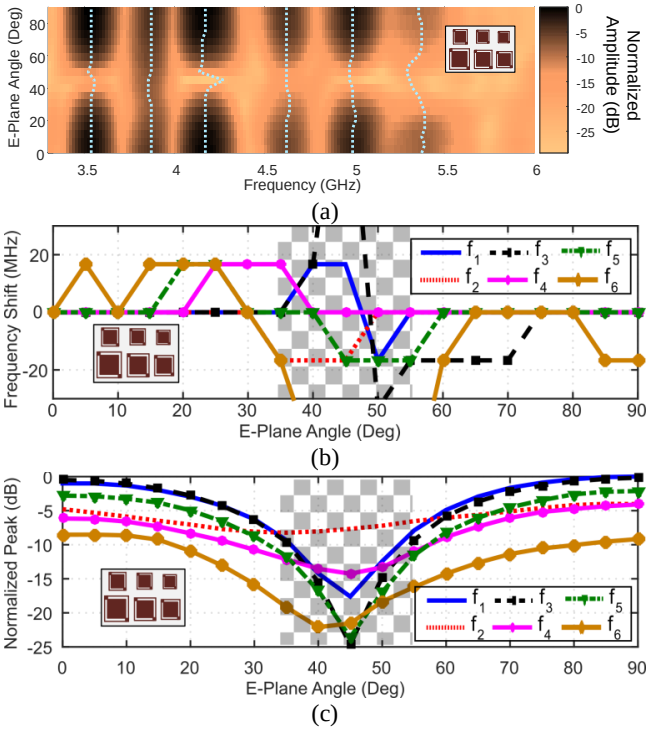

FIGURE 17. (a) Measured frequency-domain response of Design A tag 1 as a function of the E-plane angle. In light blue: Detected resonant frequency peaks. (b) Frequency shift of each resonance as a function of the E-plane angle. (c) Normalized amplitude of the peaks as a function of the E-plane angle. Tag-reader distance: 20 cm, inside an anechoic chamber.

The frequency shift is due to multiple factors: (i) the reduction of the tag RCS in a depolarizing approach with the angle of observation, (ii) the contribution of the environment with the multipath, (iii) the interaction between the tag backscattered signal and the adjacent objects such as the support used to fix the tag, and (iv) the temporal separation approach in post-processing. The tag RCS variation with the angle of observation has been studied in [39]; it decreases to about 10 dB at an angle variation of 35° with respect to the most favorable case and is also shown in Figs. 17-18. The depolarizing approach helps to reduce the multipath but it is still present. All these phenomena reduce the reader's S/N ratio and the peak detection becomes cumbersome or sometimes impossible. Thus, the frequency shift is not a physical phenomenon due to a variation of tag's resonance frequencies but a limitation of the setup comprising the reader, the environment, and post-processing. The contribution of post-processing by temporal separation technique at the frequency shift is due to the reduction of frequency resolution once the STFT is applied on the tag measurement. As expected from Fig. 17(b), the frequency shift is more important at the higher frequencies where the quality factor of the REPs is lower, reducing the S/N ratio at the reader's input.

For comparison purposes, a dual-layer depolarizing tag based on dual-L dipoles with ground plane [8] was measured (see Fig. 18). This tag is more robust and has a greater quality factor than Design A, at the cost of a two-layer structure. Again, the observation is that the region with more frequency shift is the same as with a single-layer tag, that is close to 45º.

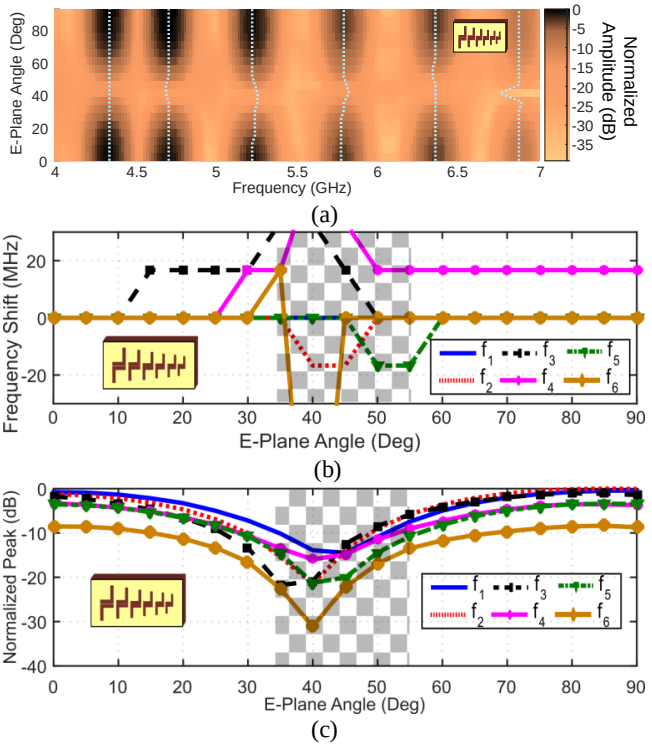

FIGURE 18. (a) Measured frequency-domain response of a high Q-factor depolarizing tag with ground plane [8] as a function of the E-plane angle. In light blue: detected resonant frequency peaks. (b) Frequency shift of each resonance as a function of the E-plane angle. (c) Normalized amplitude of the peaks as a function of the E-plane angle. Tag-reader distance: 20 cm, inside an anechoic chamber.

C. ROTATION IN H-PLANE

The tags were at first placed normal to the reader's antennas so as to maximize the tag's RCS, after the tag response was analyzed for an angle of rotation in H-plane up to 180°. The measured frequency-domain response as a function of the H-plane angle for Design A tag 1 is shown in Fig. 19. As it has been performed in Section V (B), the corresponding frequency shifts and normalized amplitude peaks are also shown. Because the tag does not have a ground plane, it can be read at 180º as well as at 0º. The worst case is close to 90º, where the tag is read perpendicularly to the reader's antennas, and its RCS is minimal. The frequency shift is ±50 MHz for all the resonators and angles.

The case for the dual-L depolarizing tag with ground plane is shown in Fig. 20. Since the ground plane is facing the

reader, the tag is only correctly read between 0º and 90º [see Fig. 20(b)], as expected. In the margin of 0º - 90º, the measured frequency shift is below ± 25 MHz. For angles greater than 90º, the frequency peaks cannot be correctly detected, due to the low S/N ratio.

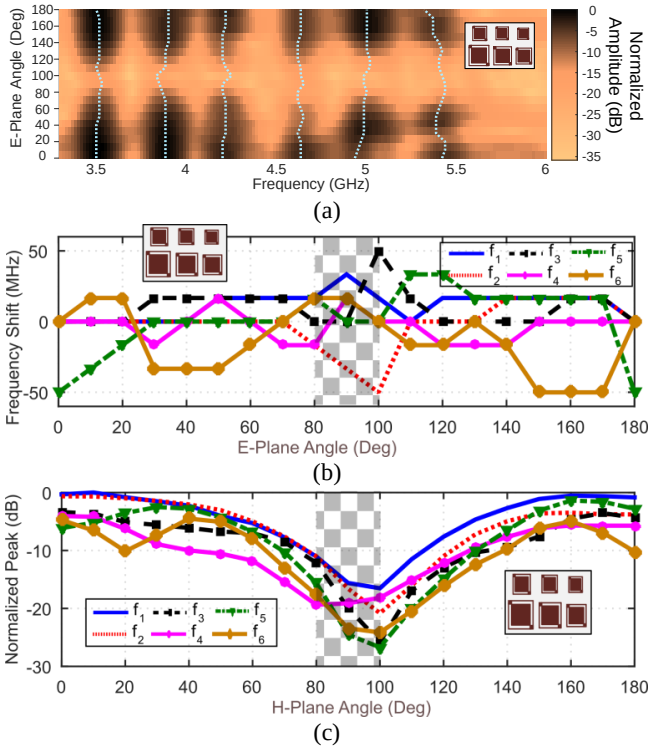

FIGURE 19. (a) Measured frequency-domain response of Design A tag 1 as a function of the H-plane angle. In light blue: Detected resonant frequency peaks. (b) Frequency shift of each resonance as a function of the H-plane angle. (c) Normalized amplitude of the signal peaks as a function of the H-plane angle. Tag-reader distance: 20 cm, inside an anechoic chamber.

All distances from tag and reader antenna are in near field radiating zone (Fresnel zone). However, the measurements even in Fresnel zone are repeatable with good accuracy.

VI. CONCLUSION

This work has proposed two different single-layer designs of chipless frequency-coded RFID tags based on the depolarizing principle and REP approach. In the direction of the industrialization of the chipless technology, the tags have been realized on plastic substrate with additive fabrication processes. It has been demonstrated that the proposed tag designs, in combination with temporal separation techniques, can be read with a single measurement. As it has been shown, this was not possible with co-polarization designs. The single measurement was possible as a result of the depolarizing principle, which has been applied for the first time on the design of a single-layer tag based on REP approach. This is a significant improvement for real case scenarios where robust readings are needed. The proposed designs have also been tested with a proof-of-concept tag commercially manufactured on paper, showing that the lower frequencies of the UWB spectrum can be detected. A study on the incidence angle both in E and H planes has been performed for the proposed tags and similar existing dual-layer designs. It has been shown that the proposed tags can be read at most tag-reader polarization angles.

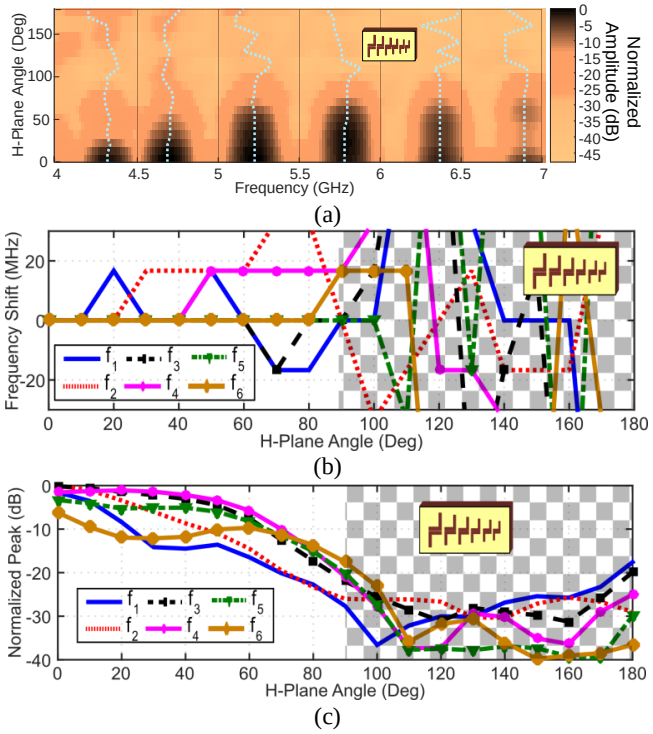

FIGURE 20. (a) Measured frequency-domain response of a high Q-factor depolarizing tag with ground plane [8] as a function of the H-plane angle. In light blue: Detected resonant frequency peaks. (b) Frequency shift of each resonance as a function of the H-plane angle. (c) Normalized amplitude of the signal peaks as a function of the H-plane angle. Tag-reader distance: 20 cm, inside an anechoic chamber.

REFERENCES

[1] E. Perret, *Radio Frequency Identification and Sensors: From RFID to Chipless RFID*. John Wiley & Sons, 2014.

[2] S. Preradovic and N. C. Karmakar, "Chipless RFID: Bar Code of the Future," *IEEE Microw. Mag.*, vol. 11, no. 7, pp. 87–97, Dec. 2010.

[3] A. Vena *et al.*, "Design of Chipless RFID Tags Printed on Paper by Flexography," *IEEE Trans. Antennas Propag.*, vol. 61, no. 12, pp. 5868–5877, Dec. 2013.

[4] M. Borgese, F. A. Dicandia, F. Costa, S. Genovesi, and G. Manara, "An Inkjet Printed Chipless RFID Sensor for Wireless Humidity Monitoring," *IEEE Sensors J.*, vol. 17, no. 15, pp. 4699–4707, Aug. 2017.

[5] D. Dardari and R. D'Errico, "Passive Ultrawide Bandwidth RFID," in *Proc. IEEE Global Telecommun. Conf.*, 2008, pp. 1–6.

[6] S. Preradovic, I. Balbin, N. C. Karmakar, and G. F. Swiegers, "Multiresonator-Based Chipless RFID System for Low-Cost Item Tracking," *IEEE Trans. Microw. Theory Techn.*, vol. 57, no. 5, pp. 1411–1419, May 2009.

[7] R. S. Nair and E. Perret, "Folded Multilayer C-Sections With Large Group Delay Swing for Passive Chipless RFID Applications," *IEEE Trans. Microw. Theory Techn.*, vol. 64, no. 12, pp. 4298–4311, Dec. 2016.

[8] A. Vena, E. Perret, and S. Tedjni, "A Depolarizing Chipless RFID Tag for Robust Detection and Its FCC Compliant UWB Reading System," *IEEE Trans. Microw. Theory Techn.*, vol. 61, no. 8, pp. 2982–2994, Aug. 2013.

[9] M. Khaliel, A. El-Awamry, A. F. Megahed, and T. Kaiser, "A Novel Design Approach for Co/Cross-Polarizing Chipless RFID Tags of High Coding Capacity," *IEEE J. Radio Freq. Identification*, vol. 1, no. 2, pp. 135–143, 2017.

[10] A. Vena, E. Perret, and S. Tedjini, "Design of Compact and Auto-Compensated Single-Layer Chipless RFID Tag," *IEEE Trans. Microw. Theory Techn.*, vol. 60, no. 9, pp. 2913–2924, Sep. 2012.

[11] O. Rance, E. Perret, R. Siragusa, and P. Lemaitre-Auger, *RCS Synthesis for Chipless RFID: Theory and Design*. Elsevier, 2017.

[12] R. A. Romero, R. S. Feitoza, C. R. Rambo, and F. R. Sousa, "A low-cost passive wireless capacitive sensing tag based on split-ring resonator," in *Proc. IEEE Int. Instrum. Meas. Techn. Conf. (I2MTC)*, 2015, pp. 434–439.
[13] A. Vena, E. Perret, D. Kaddour, and T. Baron, "Toward a Reliable Chipless RFID Humidity Sensor Tag Based on Silicon Nanowires," *IEEE Trans. Microw. Theory Techn.*, vol. 64, no. 9, pp. 2977–2985, Sep. 2016.
[14] M. A. Islam and N. C. Karmakar, "Compact Printable Chipless RFID Systems," *IEEE Trans. Microw. Theory Techn.*, vol. 63, no. 11, pp. 3785–3793, 2015.
[15] M. A. Islam and N. C. Karmakar, "A Novel Compact Printable Dual-Polarized Chipless RFID System," *IEEE Trans. Microw. Theory Techn.*, vol. 60, no. 7, pp. 2142–2151, 2012.
[16] M. Zhonghua and J. Yanfeng, "High-Density 3D Printable Chipless RFID Tag with Structure of Passive Slot Rings," *Sensors*, vol. 19, no. 11, p. 2535, 2019.
[17] M. A. Islam, Y. Yap, N. Karmakar, and A. K. M. Azad, "Orientation independent compact chipless RFID tag," in *Proc. IEEE Int. Conf. RFID-Technol. Appl. (RFID-TA)*, Nice, France, 2012, pp. 137–141.
[18] N. Tariq *et al.*, "Orientation Independent Chipless RFID Tag Using Novel Trefoil Resonators," *IEEE Access*, vol. 7, pp. 122398–122407, 2019.
[19] V. Sharma, S. Malhotra, and M. Hashmi, "Slot Resonator Based Novel Orientation Independent Chipless RFID Tag Configurations," *IEEE Sensors J.*, vol. 19, no. 13, pp. 5153–5160, 2019.
[20] M. A. Islam and N. C. Karmakar, "Real-World Implementation Challenges of a Novel Dual-Polarized Compact Printable Chipless RFID Tag," *IEEE Trans. Microw. Theory Techn.*, vol. 63, no. 12, pp. 4581–4591, 2015.
[21] F. Costa *et al.*, "A Depolarizing Chipless RF Label for Dielectric Permittivity Sensing," *IEEE Microw. Wireless Compon. Lett.*, vol. 28, no. 5, pp. 371–373, 2018.
[22] N. C. Karmakar, M. Zomorrodi, and C. Divarathne, *Advanced Chipless RFID: MIMO-Based Imaging at 60 GHz - ML Detection*. Hoboken, NJ, USA: Wiley, 2016.
[23] A. Ramos, E. Perret, O. Rance, S. Tedjini, A. Lázaro, and D. Girbau, "Temporal Separation Detection for Chipless Depolarizing Frequency-Coded RFID," *IEEE Trans. Microw. Theory Techn.*, vol. 64, no. 7, pp. 2326–2337, Jul. 2016.
[24] C. Cho, H. Choo, and I. Park, "Broadband RFID tag antenna with quasi-isotropic radiation pattern," *Electron. Lett.*, vol. 41, no. 20, pp. 1091-1092(1), 2005.
[25] A. Ramos, D. Girbau, and A. Lazaro, "Influence of materials in time-coded chipless RFID tags characterized using a low-cost UWB reader," in *Proc. 42nd European Microw. Conf.*, 2012, pp. 526–529.
[26] D. M. Pozar, *Microwave Engineering*, 2nd ed. New York: Wiley, 1998.
[27] R. C. Hansen, "Relationships between antennas as scatterers and as radiators," *Proc. IEEE*, vol. 77, no. 5, pp. 659–662, 1989.
[28] J. Huang, "Microstrip Antennas: Analysis, Design, and Application," in *Modern Antenna Handbook*, Wiley, 2007, pp. 157–200.
[29] O. Rance, R. Siragusa, P. Lemaître-Auger, and E. Perret, "Contactless Characterization of Coplanar Stripline Discontinuities by RCS Measurement," *IEEE Trans. Antennas Propag.*, vol. 65, no. 1, pp. 251–257, Jan. 2017.
[30] O. Rance, R. Siragusa, P. Lemaitre-Auger, and E. Perret, "Toward RCS Magnitude Level Coding for Chipless RFID," *IEEE Trans. Microw. Theory Techn.*, vol. 64, no. 7, pp. 2315–2325, Jul. 2016.
[31] A. Vena, E. Perret, and S. Tedjini, "A Fully Printable Chipless RFID Tag With Detuning Correction Technique," *IEEE Microw. Wireless Compon. Lett.*, vol. 22, no. 4, pp. 209–211, Apr. 2012.
[32] "Conductive Inkjet Technology." [Online]. Available: https://www.uk-cpi.com. [Accessed: 20-Sep-2017].
[33] S. B. Cohn, "Slot Line on a Dielectric Substrate," *IEEE Trans. Microw. Theory Techn.*, vol. 17, no. 10, pp. 768–778, 1969.
[34] R. Rezaiesarlak and M. Manteghi, "Short-Time Matrix Pencil Method for Chipless RFID Detection Applications," *IEEE Trans. Antennas Propag.*, vol. 61, no. 5, pp. 2801–2806, May 2013.
[35] C. E. Baum, E. J. Rothwell, K. M. Chen, and D. P. Nyquist, "The singularity expansion method and its application to target identification," *Proc. IEEE*, vol. 79, no. 10, pp. 1481–1492, Oct. 1991.
[36] R. Rezaiesarlak and M. Manteghi, *Chipless RFID: Design Procedure and Detection Techniques*. Springer International Publishing, 2014.
[37] M. Khaliel, M. El-Hadidy, and T. Kaiser, "Printable depolarizing chipless RFID tag based on DGS resonators for suppressing the clutter effects," in *Proc. 9th European Conf. Antennas Propag. (EuCAP)*, 2015, pp. 1–5.
[38] O. Rance, R. Siragusa, P. Lemaître-Auger, and E. Perret, "RCS magnitude coding for chipless RFID based on depolarizing tag," in *Proc. IEEE MTT-S Int. Microw. Symp. Dig.*, Phoenix, USA, 2015, pp. 1–4.
[39] M. Garbati, E. Perret, R. Siragusa, and C. Halopè, "Toward Chipless RFID Reading Systems Independent of Tag Orientation," *IEEE Microw. Wireless Compon. Lett.*, vol. 27, no. 12, pp. 1158–1160, Dec. 2017.